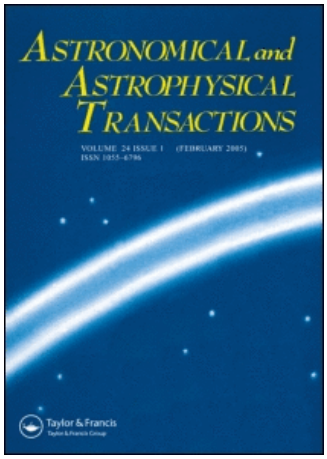

Astronomical & Astrophysical Transactions
The Journal of the Eurasian Astronomical Society
Publication details, including instructions for authors and subscription information:
http://www.informaworld.com/smpp/title~content=t713453505

Analyses and modelling of coronal holes observed by CORONAS-1. I. Morphology and magnetic field configuration

V. Obridko [a]; V. Formichev [a]; A. F. Kharshiladze [a]; I. Zhitnik [b]; V. Slemzin [b]; D. Hathaway [c]; S. T. Wu [d]
[a] IZMIRAN Institute, Russia
[b] P. N. Ledebev Physics Institute, Russia
[c] SSL/NASA/Marshall Space Flight Center, AL, USA
[d] CSPAR/University of Alabama in Huntsville, Huntsville, AL, USA

Online Publication Date: 01 June 2000
To cite this Article: Obridko, V., Formichev, V., Kharshiladze, A. F., Zhitnik, I., Slemzin, V., Hathaway, D. and Wu, S. T. (2000) 'Analyses and modelling of coronal holes observed by CORONAS-1. I. Morphology and magnetic field configuration', Astronomical & Astrophysical Transactions, 18:6, 819 - 828
To link to this article: DOI: 10.1080/10556790008208176
URL: http://dx.doi.org/10.1080/10556790008208176

Astronomical and Astrophysical Transactions, 2000, Vol. 18, pp. 819–828
Reprints available directly from the publisher
Photocopying permitted by license only

ANALYSES AND MODELLING OF CORONAL HOLES OBSERVED BY CORONAS-1. I. MORPHOLOGY AND MAGNETIC FIELD CONFIGURATION

V. OBRIDKO[1], V. FORMICHEV[1], A. F. KHARSHILADZE[1], I. ZHITNIK[2], V. SLEMZIN[2], D. HATHAWAY[3], and S. T. WU[4]

[1] *IZMIRAN Institute, Russia*
[2] *P. N. Ledebev Physics Institute, Russia*
[3] *SSL/NASA/Marshall Space Flight Center, AL 35812 USA*
[4] *CSPAR/University of Alabama in Huntsville, Huntsville, AL 35899 USA*

(Received September 30, 1998)

Two low-latitude coronal holes observed by CORONAS-1 in April and June 1994 are analysed together with magnetic field measurements obtained from Wilcox and Kitt Peak Solar Observatories. To estimate the comparable temperature of these two coronal holes, the YOHKOH observations are also utilized. Using this information, we have constructed three-dimensional magnetic field lines to illustrate the geometrical configuration of these coronal holes. The calculated synoptic maps are used to determine the existence of closed and open field regions of the hole. Finally, we have correlated the characteristics of two coronal holes with the observed solar wind speed. We found that the brighter coronal hole has a high-speed solar wind, and the dimmer coronal hole has a low-speed solar wind.

KEY WORDS Sun-coronal holes, solar wind

1 INTRODUCTION

CORONAS-1 (Oraevsky *et al.*, 1990) was launched on March 2, 1994. During the mission period (March 12, 1994–July 5, 1995), a series of solar XUV images was obtained by means of the TEREK-C telescope array. The design of the telescope and an overview of the observations are described by Sobelman *et al.* (1996).

This TEREK-C array incorporates two XUV telescopes – MX and HR. The solar images described here were obtained by the MX-telescope in two channels 17.5 and 30.4 nm with spatial resolution up to 5″. The optical design of the MX telescope is based on a Herschelian configuration. It has spherical multilayer mirrors with diameters of 30 mm and focal lengths of 800 mm with Mo–Si coatings having

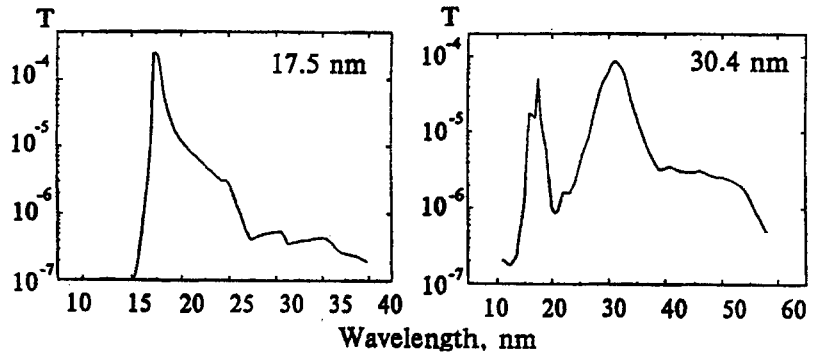

Figure 1 Throughput of the TEREK-C MX telescope for the 17.5 and 30.4 nm spectral channels (a product of the filter transmittance, the mirror reflectivity and quantum efficiency of the image detector).

periods corresponding to their spectral bands. The mirrors were switched by a shutter; images in the focal plane were registered in turn by the same detector which includes a two-stage open-type election intensifier and CCD-matrix. Spectral selection is provided by the reflection of multilayer mirrors and the bandpass of thin film filters, placed at the input entrance (prefilters) and in front of the detector (quantum efficiency of the detector is a flat function). The spectral dependencies of the throughput for the 17.5 and 30.4 nm channels are shown in Figure 1.

Estimations based on calculations by Landini and Fossi (1990) of solar spectra and differential emission measure models of Dere and Mason (1993) show that the intensity observed in the 17.5 nm spectral band is mostly due to coronal Fe OX–XI ion lines with wavelengths from 17.1 to 18.4 nm and $T_{\rm exc}$ = 1–2 × 10^6 K. The main contributions to the signal in the 30.4 nm channel is from the He II 30.4 nm resonance line with $T_{\rm exc}$ = 0.8–10^5 K which may be attributed to the transition layer. But coronal lines also contribute a significant part of the intensity in this channel: there are Fe IX–XII lines in the 17–19 nm range (in the second interference reflection maximum of multilayer coating), Si XI line 30.35 nm. Si VIII line 31.7 nm and Fe XVI line 33.5 nm. For typical coronal holes these coronal lines may contribute up to 40% of the total emission. These lines have temperatures of excitation in the range T = 0.6–2.5 × 10^6 K, that is approximately the same as in the 17.5 nm channel. We assume that pictures obtained in the 17.5 nm channel describe the structure of the plasma in the inner corona. At the same time the differences in pictures in the 30.4 and 17.5 nm channels may be attributed to the He II line which characterizes the transition region.

The TEREK solar images were compared with images of the hotter corona in the 0.3–4.5 nm X-ray band ($T_{\rm exc}$ = 3–5 × 10^6 K) obtained by the SXT telescope on board the YOHKOH satellite. In contrast to the YOHKOH data, the TEREK pictures show the structure of solar plasma in the altitude region characterized by the highest gradients of temperature and magnetic field.

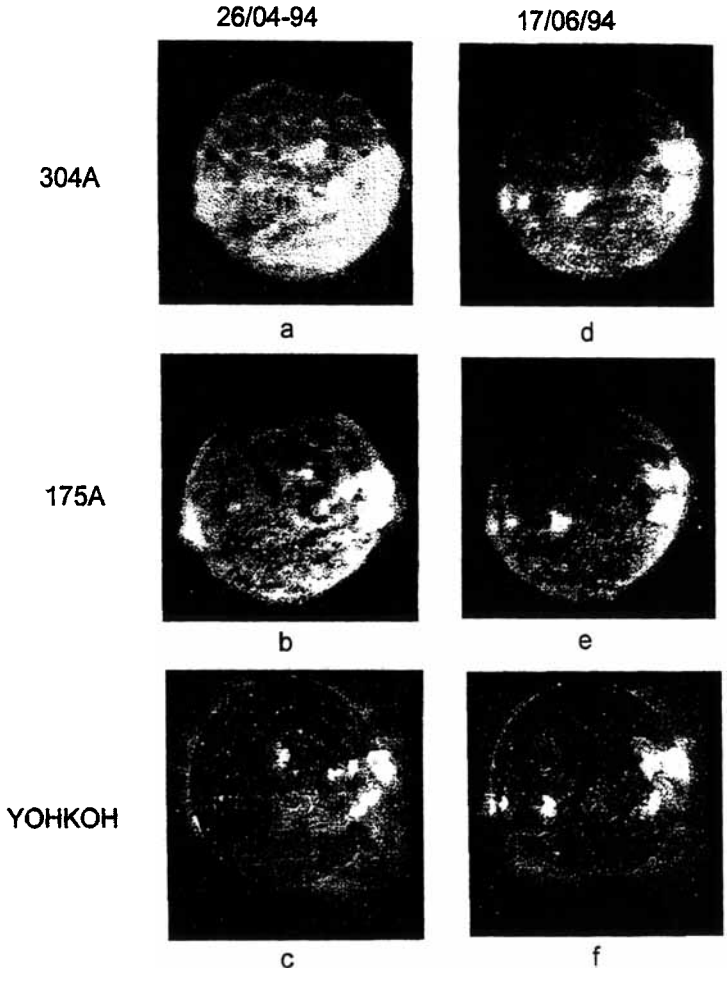

Figure 2 Two sets of images obtained with TEREK (*a*, *b*, *d*, *e*) and YOHKOH (*c*, *f*).

2 EXPERIMENTAL DATA AND THEIR REPRESENTATION

During three solar rotations, XUV CORONAS observations were carried out with time intervals from tens of seconds to 2–3 days. We selected two sets of images obtained in April 26 and June 17, 1994 in which the solar disk images showed large low-latitude coronal holes seen with high contrast at the background of relatively intense solar activity (Figure 2*a*, *b*, *d*, *e*). In Figure 2 *c*, *f* corresponding YOHKOH images are shown. The original TEREK images are 1024×1152 pixels (angular scale $5''$/pixel) or 460×576 pixels ($10''$/pixel); YOHKOH images are 512×512 pixel ($4.8''$/pixel). For uniformity, the images were reduced to 256×256 pixels with a scale of $10''$/pixel.

For detailed comparisons of TEREK and YOHKOH images with each other and with computed magnetic field configurations, daily images of each kind for April and June were transferred into photometric synoptic charts which include latitudes $\pm 70°$. Polar regions with latitudes higher than 70° were not included in the charts because of large geometric distortion.

Such charts were built using a program written in IDL as follows. First, according to the time of registration, central zones in each image were cut with widths allowing for continuous connection. Then, each part was transformed from spherical to Mercator coordinates by bilinear interpolation. Finally, five intensity ranges were selected and marked as levels with different colours. The lowest level represents a coronal hole interior. The second and third levels correspond to the ranges of mean and enhanced disk brightness (not including bright active regions). The two highest levels represent the brightness of weak and bright active regions. Scale brightness is the same for all the images. It is important to note that intensities of the primary images (before transformation of coordinates) were scaled so that the brightest active region will be at the 255 level. Because intensities of active regions are changing in time, the whole brightness scale is also oscillating and some regions at neighbouring pictures do not always coincide. To fix the coronal hole boundaries, we have used observations of YOHKOH.

To obtain the three-dimensional magnetic field configuration, we use the line-of-sight magnetic field measurements from the Wilcox Solar Observatory from which it is assumed that all components of the magnetic field at any point in a spherical layer annulus from the photosphere to the so-called source surface can be calculated under the potential field approximation by using line-of-sight magnetic field observations in the photosphere. The source surface is, by definition, a sphere where all field lines are radial. It is assumed to exist at a distance $R_s = 2.5R_0$ from the centre the Sun. At the present, the source surface hypothesis does not bring about errors in the analysis because we are interested in the field on the solar surface (i.e. $R = R_0$) for the determination of the coronal hole boundary. The equations used to calculate the magnetic field components are written as follows:

$$B_r = \sum P_n^m(\cos\theta)(g_{nm}\cos m\varphi + h_{nm}\sin m\varphi) \times \left((n-1)\left(\frac{R_0}{R}\right)^{n+2} - \left(\frac{R_0}{R}\right)^{n-1} c_n\right), \quad (1)$$

$$B_\theta = -\sum \frac{\partial P_n^m(\cos\theta)}{\partial\theta}(g_{nm}\cos m\varphi + h_{nm}\sin m\varphi) \times \left(\left(\frac{R_0}{R}\right)^{n+2} + \left(\frac{R_0}{R_s}\right)^{n-1} c_n\right), \quad (2)$$

$$B_\varphi = -\sum \frac{m}{\sin\theta} P_n^m(\cos\theta)(g_{nm}\cos m\varphi + h_{nm}\sin m\varphi) \times \left(\left(\frac{R_0}{R}\right)^{n+2} + \left(\frac{R_0}{R_s}\right)^{n-1} c_n\right). \quad (3)$$

Here, $0 \leq m \leq n \leq N$ (conventionally we set $N = 9$), $c_n = (R_0/R_s)^{n+2}$, P_n^m are the associated Legendre polynomials and g_{nm} and h_{nm} are the coefficients of spherical harmonic analysis deduced from the original observational data using the potential field model. These coefficients are tabulated (Hoeksema and Schrerrer, 1986; Hoeksema, 1991) from May 1976 until January 1991. For later periods, they were directly calculated from the data that we received from T. Hoeksema.

A new sophisticated software facility has been developed. It yields the synoptic charts of the source surface field, the maps of the data and the calculated line-of-sight fields on the photosphere surface, and the differences between the two maps. Then, the synoptic charts of the radial and horizontal vector components are calculated for each height at the user's demand. The horizontal field can be represented either as isolines, or as vectors with a length proportional to the field intensity. Any date can be taken for the centre of the synoptic chart.

At the next stage, the field line at every point on the chart is analysed to find out whether it is open (i.e. reaches the source surface) or closed (i.e. returns to its original height). For this purpose, the following procedure is applied. Choose the 'test level' in the solar atmosphere from 1.00 to 2.50. On the synoptic chart for each component, mark 'X' at the points intersected by the closed field lines, and 'O' at the points intersected by the open ones. Note that the levels where the field is calculated may not coincide with the 'test level'. For example, we can analyse the field lines at the 1.1 level and superimpose the obtained result on the source surface. Another possible way is as follows: starting from the source surface, where the field lines are open by definition and the network knots are evenly spaced, we trace every field line up to the chosen height, and find the coordinates at that point. The ends of the field lines at that level will not be evenly spaced, but will rather determine the 'open configuration' regions. The density of the points at the test level will reveal the 'over-radiality' characteristics of the coronal holes. In addition, a field line pattern can be obtained for every rotation.

3 PHYSICAL INTERPRETATION OF THE OBSERVATIONS

The results of more detailed comparisons of the coronal hole structure in April with the YOHKOH and CORONAS data are represented in Figures 3–5. All these figures have been plotted using the same procedure. Note that the photometric maps are inverse intensity images (negatives) – the coronal holes are seen as light features.

Figure 3*a* illustrates a photometric map from YOHKOH, with the superimposed radial magnetic field in the photosphere. Isolines are drawn at 0, ±100, 200, 500, 1000, and 2000 μT. The centre of the picture corresponds to 22 April 1994. The same picture shows the starting points of the field lines at the photospheric level. Open lines are marked with O and closed with X. In other words, the field line starting point O reaches the source surface.

Figure 3*b* represents the same photospheric map with superimposed radial field and open/closed configurations at the altitude of $1.1R_0$ from the centre of the Sun. Isolines are drawn at 0, ±62, 124, 310, 621, and 1242 μT.

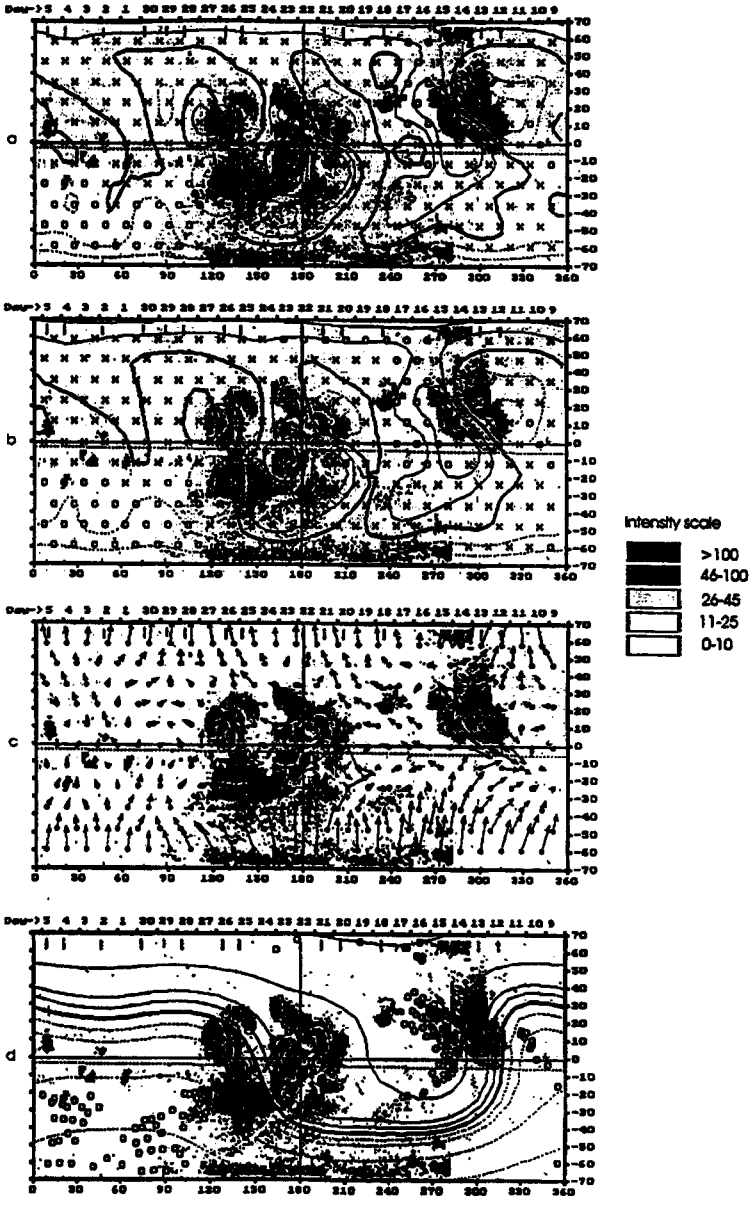

Figure 3 Photometric map from YOHKOH for 22 April 1994 with superimposed synoptic chart of magnetic field parameters: the contour represents the total magnetic field strength, the heavy dark lines are the neutral line, the thin solid line is the positive polarity, the thin dashed line is the negative polarity, the symbol X indicates the closed field line, the symbol O indicates the open field line and the arrow indicates the tangential field line with strength and direction at (*a*) photosphere, (*b*) $1.1R_s$, (*c*) $1.1R_s$ and (*d*) source surface ($2.5R_s$).

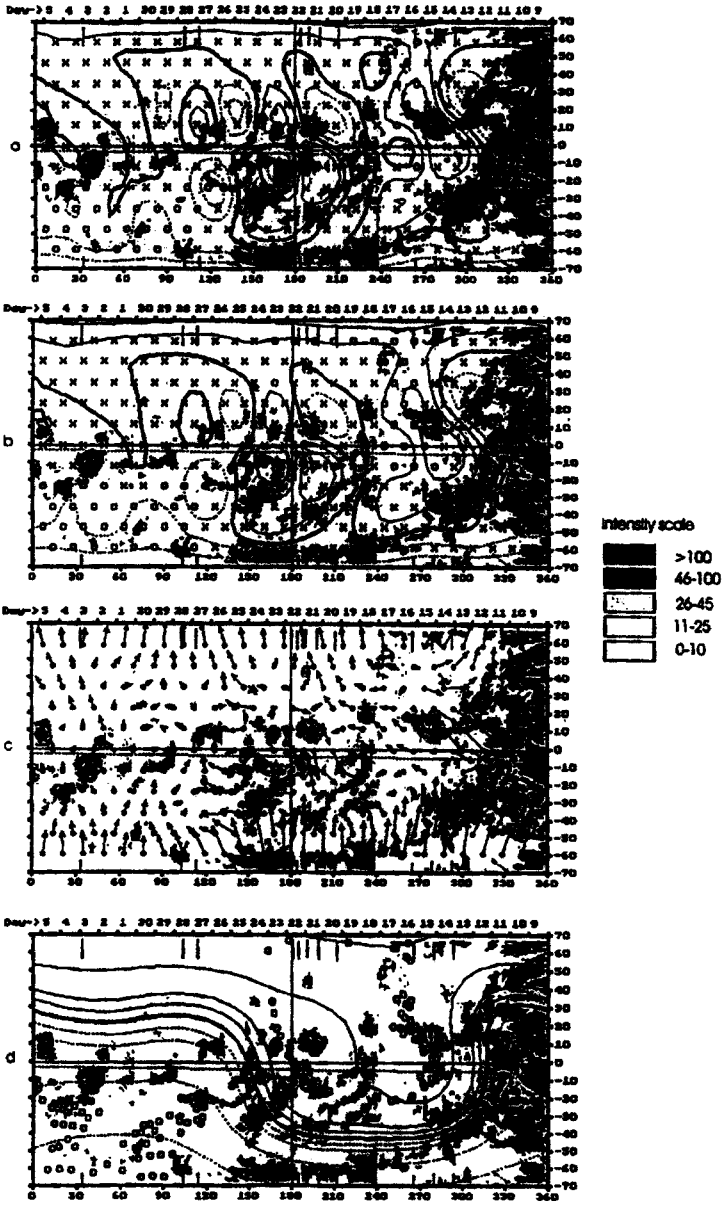

Figure 4 Photometric map from CORONAS observed in Fe IX–XI for 22 April 1994 with superimposed synoptic chart of magnetic field parameters as indicated in Figure 3.

Figure 3*c* shows the same photospheric map with superimposed tangential solar magnetic field computed at $1.1R_0$. The maximum length of the vector is 164.1 μT.

In Figure 3*d*, the photometric map is matched with the source surface magnetic field. Isolines are drawn at levels, 0, $\pm$1, 2,5, 10, and 20 μT. The same map

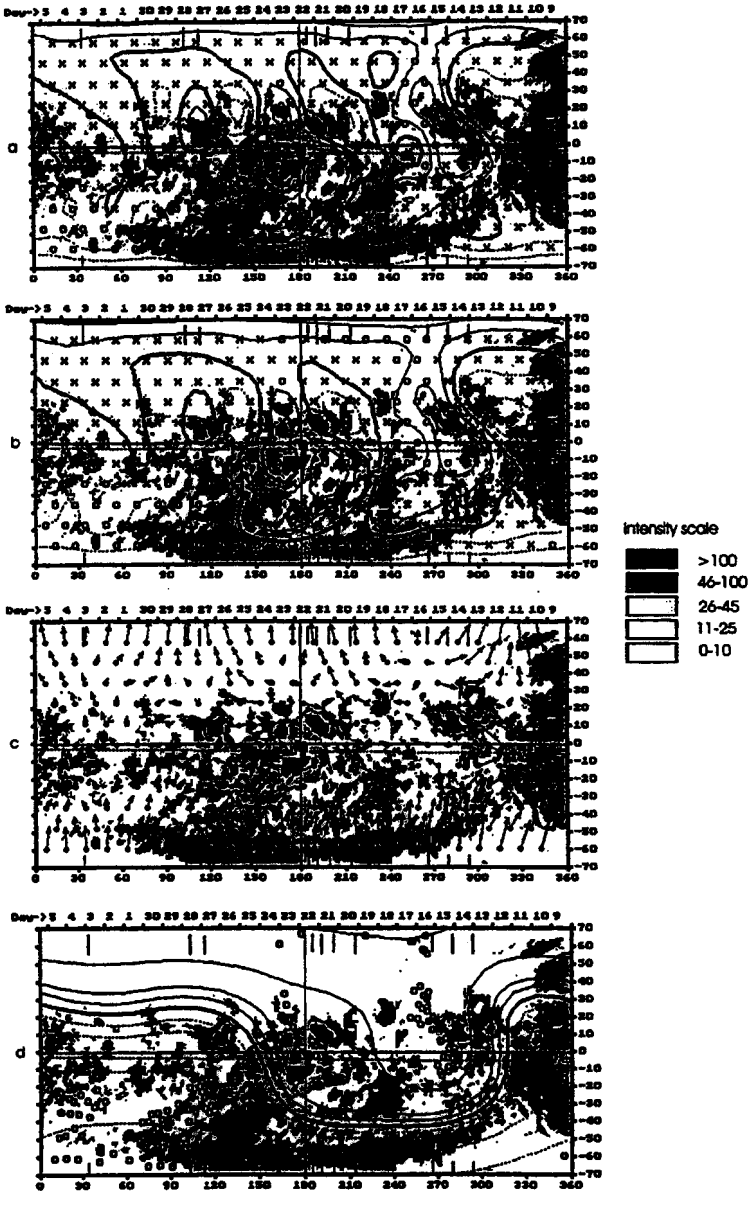

Figure 5 Photometric map from CORONAS observed in He II with superimposed synoptic chart of magnetic field parameters as indicated in Figure 3.

illustrates the ends of open field lines at the photosphere level computed by the second method. One can see a cluster of open field lines on the boundary of the coronal hole.

Figures 4 and 5 are plotted in a similar manner, but the magnetic field characteristics are superimposed on the photometric maps obtained from CORONAS observations in Fe IX–XI (Figure 4) and He II (Figure 5). The coronal hole observed on June 14, 1994 has identical characteristics, which we shall not repeat here.

4 CONCLUDING REMARKS

From this analysis of the observed coronal hole by CORONAS-I, we find the following features.

(a) All YOHKOH coronal holes agree in location, size, and shape with the open configuration regions. It is particularly pronounced when we analyse the network of the field line distribution by specifying the symbol X (closed) and O (opened) configurations seen in Figures 3*a*, *b*, 4*a*, *b*, and 5*a*, *b*.

(b) The contrast of coronal holes (the ratio of minimum brightness in the hole to mean disk brightness excluding active regions) is very high (> 40) in YOHKOH images, two times less (15–20) in 175 A TEREK images and about 5–7 in the 304 A TEREK images. This proves that in the TEREK spectral bands we really see the deepest parts of coronal holes.

(c) The photometric interior structure of the YOHKOH coronal holes is sufficiently uniform, whereas the structure in He II and Fe IX–XI is highly inhomogeneous and has many details. One can see coronal hole 'nuclei' – relatively small dark features seen in the negative images of Figures 4*d* and 5*d*. The zones of clustered open field lines (i.e. the regions of particularly pronounced super-radial expansion) are observed in the vicinity of these nuclei, but do not always coincide with the nuclei (Figures 4*d* and 5*d*). In addition, the maps of transverse fields show that these 'nuclei' occur in zones where the transverse field vanishes or the opposite-directed transverse field links up, which may imply the existence of a shear.

Figure 6 establishes a relation between the solar wind velocity and coronal holes. As seen in the preliminary analysis, the coronal hole observed in April was brighter in the TEREK images than the hole observed in June. Figure 6 represents the solar wind velocities during three passages of these coronal holes. One can readily see that the velocity is much higher in the 'bright' hole. However, this conclusion must be taken with caution, because both coronal holes differ significantly in many other respects (e.g. in dimensions, stability, etc.). The detailed information concerning MHD modelling of these observations is given in paper II (Wang *et al.* 1998).

Acknowledgement

The work performed is supported by NASA Headquarters grant NAG5-6174. Three of us (VO.VF, and VS) express our sincere gratitude to our colleagues at CSPAR

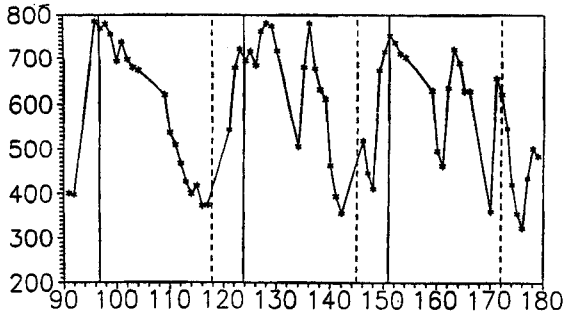

Figure 6 Solar wind velocities. Abscissa is the day of the year 1994. Solid vertical lines are the hot CH, dashed is the cold CH. The position of the CH's were displaced 4 days to account for the transport time.

(The University of Alabama in Huntsville) for their help and hospitality. Special thanks is given to the group of Dr. I. Zhinik under scientific guidance of Prof. I.I. Sobelman for the observations of the TEREK-C telescope which was designed by the P. N. Lebedev Physics Institute and the Lockheed Palo Alto Research Laboratory, the National Astronomical Observatory in Japan, and the University of Tokyo with the support of NASA and ISAS for observations observed by the X-ray telescope on-board the YOHKOH satellite.

References

Dere, K. P. and Mason, H. E. (1993) *Solar Phys.*, **144**, 217.

Hoeksema, T.,(1991) *The Solar Magnetic Field 1985 through 1990'*, Report CSSA – ASTRO-91-01.

Hoeksema, T. and Scherrer, P. H. (1986) *The Solar Magnetic Field 1976 through 1985*, UAG094.

Landrini, M. and Fossi, M. B. (1990) *Astron. Astrophys. Suppl. Ser.* **82**, 229.

Oraevsky, V. N., Fomichev, V. V., and Zhugzhda, Yu. D. (1990) *Proc. Symposium on Npbeyama Radioheliograph*, p. 132.

Sobelman, I.I., Zhitnik, I. A., Ignatiev, A. P. *et al.* (1996) *Astron. J.* **22**, No. 8, 605 (in Russian).

Wang, A. H., Wu, S. T., Dryer, M., Hathaway, D., Obridko, V., Fomichev, V., Kharshiladze, A. F., Zhitnik, L., and Slemzin, V. (1998) In: *Proceedings of the SOLTEP III Symposium*, 14–18 October, 1996, *Chinese J. of Space Science*, 1998 (in press).